Pharmacokinetics and Modeling 13

Everything that can be counted does not necessarily count; everything that counts cannot necessarily be counted. (Albert Einstein)

13.1 Quantitation

Molecular imaging of radiotracer distribution by PET or SPECT following intravenous injection shows the pattern of relative uptake of radioactivity in different organs and also in different regions within any particular organ of interest. These imaging studies permit measurement of the time course of uptake and clearance of specific tracers. Quantitative measurement of the local radiotracer activity is essential to assess the local physiological function quantitatively. Semi-quantitative methods have been developed for the interpretation of routine clinical diagnostic studies. However, absolute measurement of physiologic parameters generally requires accurate measurement of radioactivity concentrations in the arterial blood and in a specific region of interest (ROI) or volume of interest (VOI) in a tissue, in order to extract quantitative information based on tracer kinetic or compartmental modeling techniques.

In PET, the count rate per voxel in the reconstructed tomographic image, in principle, is proportional to the activity concentration in a given ROI. Since the attenuation and scatter corrections are not reliable in SPECT, the count rate per voxel in a SPECT image does not necessarily reflect the true activity concentration. As a result, true quantitation with SPECT technique is not practically feasible at this time. Some of the basic principles and concepts involved in quantitative methods will be described briefly here with specific examples.

13.1.1 Standardized Uptake Value

To make the PET images quantitative, the PET camera is first calibrated using a cylindrical phantom with known radioactivity concentration (Bq mL^{-1}). The count rate per voxel (cps or cpm) is then divided by the measured system calibration factor, CF [(Bq cc^{-1})/(cps $voxel^{-1}$)], to convert cps in a given ROI to the corresponding activity concentration units, C_t (Bq cc^{-1}).

Following administration of a PET radiotracer, the image acquisition represents a sum of coincidence counts due to true, scatter, and random events. At the end of the image acquisition, the following corrections are required to make the PET data truly quantitative:

- Attenuation correction (performed using the CT scan data).
- Scatter and random correction.

S. Vallabhajosula, *Molecular Imaging and Targeted Therapy*,
https://doi.org/10.1007/978-3-031-23205-3_13

- Energy correction.
- Linearity distortion correction.
- Normalization and dead time correction.
- Dose calibrator cross calibration with PET scanner.

It is common practice in animal studies to express the biodistribution of radiotracers using the parameter, the percent injected dose per gram of tissue (%ID/g of tissue), which is calculated using the following equation.

$$\%\mathrm{ID/g} = \frac{\text{Activity in a gram of tissue}\left(C_t\right)}{\text{Injected dose}} ?100 \tag{13.1}$$

The %ID/g parameter, however, does not take into consideration the total body mass (weight) of a patient. The standardized uptake value (SUV) measured with a PET scanner is a semi-quantitative unit developed in order to include the total body weight of a patient [1–5].

$$SUV = \frac{C_t \text{ in a } ROI\left(\mathrm{MBq/cc}\right)}{\text{Injected dose } \left(\mathrm{MBq}\right)} ?\text{Body wt}\left(\mathrm{g}\right)?100 \tag{13.2}$$

$$SUV_{ROI} = A_{ROI}\left(T_S\right) / \mathrm{Conc}_S\left(T_S\right)$$

where, Conc = Dose/wt, and T_s = the time of the scan.

The SUV value, therefore, is a unitless number that normalizes the lesion uptake to the injected dose per unit of body weight. It has also been proposed that normalization of SUV based on body surface area (BSA) may improve the accuracy of SUV but, a method of normalization has not been routinely employed by most PET users. It is important to recognize that many factors (dose infiltration, serum glucose levels, total body fat, and the lesion volume) other than the metabolic status of the lesion can significantly affect the reliability of the SUV measurement in routine clinical practice. In addition, a number of factors, including regional blood flow, enzyme activity, active transport mechanisms, and binding site concentrations, may also contribute to the amount of radioactivity present in a given ROI at any given time. The SUV determination is regarded as semiquantitative since it does not consider many of these biochemical processes and all the possible contributions to overall tissue activity levels.

The quantification of [^{18}F]FDG uptake by using the maximum standardized uptake value (SUV_{max}) is the traditional PET-derived parameter used as a biomarker of glucose metabolism of several biological processes for both diagnostic and follow-up purposes. Several other parameters have also been developed such as SUV_{mean}, SUV_{peak}, SUV_{max}, or SUV_{peak} corrected for lean body mass (SUL_{max} and SUL_{peak}). Sometimes, a simple traditional parameter such as Target/Background (T/B) ratio may be utilized. It is important to optimize quantitative techniques since disease progression and response to therapy are determined based on the PET SUV values [2].

13.2 Physiological Modeling

PET and SPECT permit sequential measurements of the radioactivity distribution in vivo following intravenous administration of a radiopharmaceutical at tracer levels. The mea-

sured time-activity distribution, however, is influenced by various factors, such as blood flow, clearance from plasma, the number of specific and nonspecific binding sites, and their affinity. For a tracer to have any value in clinical practice, the uptake and distribution of the tracer must quantitatively and accurately reflect the concentration of available binding sites or the rate of some biochemical processes. The extraction of quantitative values from dynamic PET imaging data requires the fitting of the data to a mathematical model that describes the uptake and retention of the tracer in tissue. Tracer kinetic physiologic modeling provides the link between activity levels measured in a specific ROI in the functional scan and the physiologic parameters associated with the particular function being studied. The kinetic models can be classified as noncompartmental, compartmental, or distributive. With most molecular imaging radiopharmaceuticals, compartmental models have become the model of choice. These models describe mathematically using a set of differential equations, the transfer and behavior of the radiotracer between compartments, each of which represents distinct anatomic, physiologic, or biochemical space (such as capillaries, extracellular, intracellular, and receptor-bound). It is important to realize that the segmentation of the physiologic processes into these compartments is only a simple approximation to derive quantitative parameters and may not necessarily reflect real in vivo biological processes.

13.2.1 Radiotracer Binding

The radiotracers or the radioligands used in molecular imaging studies are generally assumed to bind selectively to the target site receptor (R) or an enzyme (E). The simplest model is the bimolecular reaction [6], describing the kinetics of the radioligand (L) binding with a specific receptor (R) or an enzyme (E) to form a complex, LR or LE. According to the law of mass action (Eq. 13.3), the rate of the reaction will proceed in proportion to the product of concentration of the reactants. Several equations pertinent to ligand-receptor interactions and their relationships are summarized in Fig. 13.1.

$$[\mathbf{L}]+[\mathbf{R}]\underset{k_{on}}{\overset{k_{off}}{?}}[\mathbf{RL}] \tag{13.3}$$

$$At \text{ equilibrium}, \quad \mathbf{k_{on}}[\mathbf{L}][\mathbf{R}]?\mathbf{K_{off}}[\mathbf{RL}] \tag{13.4}$$

$$\text{The equilibrium constant}, \quad \mathbf{K_D} = \mathbf{K_{off}} / \mathbf{K_{on}} \tag{13.5}$$

$$\text{The total number of receptors}, \quad \mathbf{B_{max}} = [\mathbf{R}]+[\mathbf{RL}] \tag{13.6}$$

$$\text{The concentration of bound receptors} \quad [\mathbf{RL}] = \frac{\mathbf{B_{max}}[\mathbf{L}]}{[\mathbf{L}]+\mathbf{K_D}} \tag{13.7}$$

$$\text{The Binding Potential } (BP) \quad \mathbf{BP} = \frac{\mathbf{B_{max}}}{\mathbf{K_D}} = \frac{[\mathbf{RL}]}{[\mathbf{L}]} = \frac{\mathbf{B}}{\mathbf{F}} \tag{13.8}$$

Fig. 13.1 Basic equations of ligand (L) and receptor (R) binding or interaction

$$[L] + [R] \underset{k_{off}}{\overset{k_{on}}{\rightleftharpoons}} [RL] \quad (13.3)$$

At equilibrium,

$$k_{on}[L][R] \rightleftharpoons K_{off}[RL] \quad (13.4)$$

The equilibrium constant,

$$K_D = K_{off}/K_{on} \quad (13.5)$$

The total number of receptors,

$$B_{max} = [R] + [RL] \quad (13.6)$$

The concentration of bound receptors

$$[RL] = \frac{B_{max}[L]}{[L] + K_D} \quad (13.7)$$

The Binding Potential (BP)

$$BP = \frac{B_{max}}{K_D} = \frac{[RL]}{[L]} = \frac{B}{F} \quad (13.8)$$

13.2.1.1 Binding Potential

In PET and SPECT studies with high SA radiotracers (L^*), the concentration of the bound receptors [RL^*] is very small (<5%), and the receptor concentration [R] is approximately equal to B_{max}. Under these conditions, the binding potential (BP) is defined as B_{max}/K_d and is equal to the ratio of the bound radioligand concentration to the free radioligand concentration (B/F) at equilibrium (Eq. 13.8). BP is proportional to B_{max} if K_d can be regarded as a constant [7, 8, 9].

13.2.1.2 Affinity

The affinity of a ligand for a receptor refers to the binding strength and can be expressed as a K_D or K_i value, which can be calculated from the measured IC_{50} value as shown in Fig. 13.2.

In a typical "saturation" radioligand binding assay experiment in vitro, increasing amounts of a radioligand are added to a fixed concentration of receptors, and the amount of radiotracer bound B or [RL] is measured as a function of [L]. Nonlinear regression analysis can be used to fit the data to the Eq. 13.7 in order to estimate both B_{max} and K_D (Fig. 13.3).

The IC_{50} value is also determined in vitro by measuring the competitive effect of different concentrations of the ligand of interest (10^{-12}–10^{-4} M) on the binding of a reference radioligand with known affinity and concentration to a preparation of cells or cell membranes known to express specific receptors for the ligand under investigation.

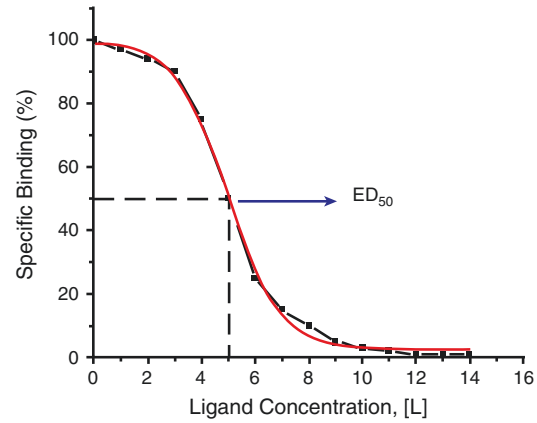

Fig. 13.2 Saturation of specific binding sites by carrier-added ligand concentration, [L]. ED_{50} can be defined as the [L], which reduces the specific binding signal by 50%. The specific binding can be determined ex vivo studies, or in vivo using MicroPET or MicroSPECT imaging

In order to obtain high contrast images, the radiotracer must have high affinity (low K_D) for its receptor. The required affinity, however, depends on the receptor concentration, B_{max}, in a given ROI. Typically, for radio labeled antagonists, high affinity in the nanomolar range is needed to obtain high contrast images.

In order to image the distribution of one specific receptor subtype, the radioligand should preferably bind only to that specific receptor with

high affinity. Certain radioligands, may have affinity for many receptor subtypes or even different receptors. Therefore, in addition to high affinity, radioligands should also have *selectivity*, which is defined as the ratio of affinity of a ligand for the receptor of interest to the affinity for each of the other receptor types.

13.2.2 Tracer Kinetics

Following intravenous administration, the radiotracer is cleared from circulation rapidly and enters a tissue compartment in which the tracer may bind to an enzyme, a specific receptor, or even undergo metabolism and subsequent intracellular trapping. For most of the radiotracers, the kinetics can be described using a maximum of three different compartments (Fig. 13.4). The first compartment is the arterial blood, in which the radiotracer may be present either as "free" species or exhibit plasma protein binding (PPB). From the arterial blood, the radiotracer passes through a second compartment (extracellular or intracellular fluid), also known as a free compartment. The third compartment is the region where the tracer is bound to either an enzyme or a specific receptor, or metabolically trapped.

In tracer kinetic modeling, certain fundamental or physiologically reasonable assumptions are usually made to minimize the number of kinetic parameters needed to improve the fit to the measured data (from imaging studies) to the physiological model or to simplify the imaging and analysis protocols. These simplifications, however, must be physically meaningful and must be validated against the complete model [8, 9].

Although most physiological and biological processes are nonlinear, the behavior (transport and or chemical reactions) of radiotracers in vivo is assumed to be linear or approximately linear due to the fact that the mass of the tracer is very small. First-order kinetics can describe the exchange of a radioligand between compartments.

- In general, the system under study is effective in a *steady state* and the administration of the radioligand does not perturb the steady state.
- Since arterial blood delivers radioligand to all tissues, the input function is always the blood time-activity concentration (TAC). Also, the radioligand can pass back and forth freely from the arterial plasma to the free compartment.
- For most radioligands, the nonspecific-binding (NSB) compartment is assumed to be in rapid

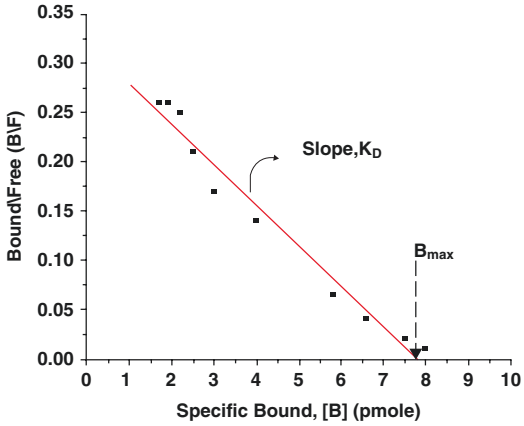

Fig. 13.3 A Scatchard plot of the ligand (L)-receptor (R) binding data in order to estimate receptor concentration (B_{max}) and affinity (K_D)

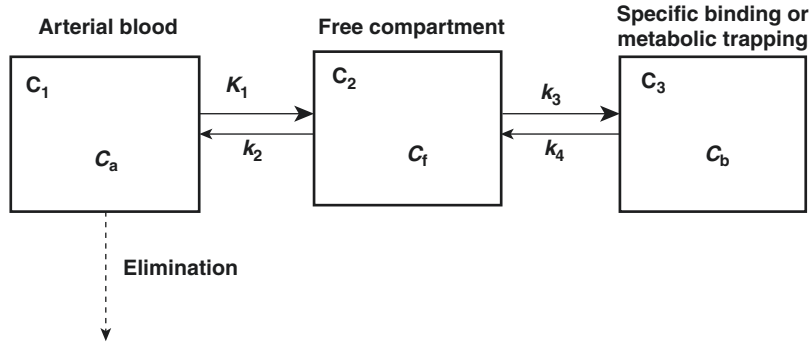

Fig. 13.4 Two and three compartment models used to describe radiotracer kinetics in vivo. Different terms used to describe the movement of radiotracer in different compartments are listed in Table 13.1

equilibrium with the free compartment and the two compartments are treated as a single compartment.

A number of parameters used in the modeling equations below and the terms used in the description of 3-compartmental model are defined in Table 13.1.

13.2.2.1 Two-Compartment Model

This model, generally, represents the movement of the radiotracer between the blood pool (C_1) into the tissue pool (C_2), as shown in Fig. 13.4. The change of tissue concentration of the radiotracer (C_t) over time is described by the following differential equation.

$$\frac{dC_t}{dt} = K_1 C_a ? k_2 C_t \qquad (13.9)$$

In the above equation, K_1 describes the speed of transfer of the ligand from the blood to the tissue and depends on the concentration of the tracer in the plasma C_a(t) and on the properties of the transport process (e.g., the activity of carrier enzyme). Because the tracer dose does not saturate the transport process, the transfer from the blood to the tissue is simply given by the product of $K_1 C_a$(t). Similarly, the transport from the tissue to the blood is given by the product of $k_2 C_t$(t).

This two-compartment (or one tissue compartment) model is generally utilized with some minor modifications in the measurement of radiotracer transport across the BBB.

The measurement rCBF is one of the major clinical applications of PET using freely diffusible radiotracers, such as [^{15}O]water. With diffusible radiotracers, the initial tracer activity in the brain is directly related to the blood flow (F) [10, 11]. Free diffusion of the tracer also leads to equilibration of C_t with that of C_v (concentration in out flowing venous blood). Thus, C_t is the same as $C_v\lambda$, where λ is the tissue/blood partition coefficient (synonymous with distribution volume) of the radiotracer. As a result, Eq. 13.9 is modified to replace K_1 with F and k_2 with F/λ, as shown below.

$$\frac{dC_t}{dt} = FC_a ? \frac{F}{?} C_t \qquad (13.10)$$

Table 13.1 Important parameters used in physiological modeling

Parameter	Description	Units
C_a	Tracer concentration in arterial blood or plasma	Bq mL^{-1}
C_f	Free tracer concentration in tissue	Bq mL^{-1}
C_t	Concentration of free tracer in tissue	Bq mL^{-1}
C_b	Concentration of tracer specifically bound to receptors, enzyme, or metabolically trapped	Bq mL^{-1}
K_1	Kinetic constant for transfer of tracer from blood to tissue ($C_a \rightarrow C_f$)	mL min^{-1} g^{-1}
k_2	Kinetic constant for transfer of tracer from tissue to blood ($C_f \rightarrow C_a$)	L min^{-1}
k_3	Kinetic constant for conversion of free tracer in tissue to specific binding or metabolic trapping ($C_f \rightarrow C_b$)	L min^{-1}
k_4	Kinetic constant for the dissociation of specifically bound or metabolically trapped tracer to free tracer in tissue ($C_b \rightarrow C_f$)	L min^{-1}
DV	Distribution volume	mL g^{-1} of tissue
B_{max}	Maximum receptor binding capacity	Mol g^{-1}
K_D	Equilibrium dissociation constant	
BP	Binding potential	mL g^{-1}
K_M	Michaelis-Menten constant (substrate concentration at half-maximum velocity)	
λ	Tissue/blood partition coefficient	
E	Tracer extraction fraction from blood (capillaries) into tissue	Unit less parameter
P	Capillary permeability for the tracer	cm min^{-1}
S	Capillary surface area	cm^2 g^{-1}

For radiotracers that are not entirely freely diffusible, the first pass extraction from the blood to the tissue is important. The transfer from the blood to the brain (K_1) is determined by the product of the blood flow (F) and tracer extraction fraction (E). The relationship between E, S, P, and F is given by the Renkin-Crone equation [12].

$$E = 1 - e^{-\frac{PS}{F}} \tag{13.11}$$

When the tracer arrives in the capillaries, some fraction of it is extracted into the tissue across the capillary walls. This unidirectional extraction fraction (E) is a unitless parameter and depends on the capillary permeability (P) for the tracer, total available capillary surface area (S), and the blood flow (F). The extraction fraction, E, will increase if S or P increases, but E will decrease if blood flow, F, increases.

13.2.2.2 Three-Compartment Model

Many radiotracers undergo metabolism (FDG, FDOPA, FLT) or are bound to specific receptors in the brain or some other tissues (Raclopride, Flumazenil, FET, Ga-DOTATOC). For most of the molecular imaging radiotracers, metabolism and specific intracellular binding are the physiological processes of interest. The dynamic behavior of many of these radiotracers in vivo is assumed to follow a standard three-compartment kinetic model (Fig. 13.4) with a single arterial input function and two tissue compartments.

Compartment C_1 represents the arterial concentration of the free, unmetabolized tracer. The passage into the tissue is considered to appear either through passive diffusion in the presence of a concentration gradient or through an active transport mechanism. Compartment C_2 is the first tissue compartment and represents an extra vascular pool of the tracer in the tissue; this tracer is available for binding or further reaction. Compartment C_3 is the concentration of the tracer that is specifically bound to the target molecule (C_b) or has undergone some chemical reaction or metabolism (C_m). The transfer of the radiotracer in these three compartments is described by the following two differential equations.

$$\frac{dC_2}{dt} = K_1 C_a - (k_2 + k_3) C_2 + k_4 C_3 \tag{13.12}$$

$$\frac{dC_3}{dt} = k_3 C_2 - k_4 C_3 \tag{13.13}$$

For radiotracers with irreversible metabolism or metabolic trapping (such as FDG and FLT), k_4 is negligibly small, and the total tissue tracer activity, $C_t(t)$, can be split into two components, the reversible free tracer, $C_f(t)$, and the trapped metabolized tracer, $C_m(t)$.

FDG Metabolism: Measurement of MRglc

The technique of measuring MRglc using FDG metabolic intracellular trapping is based on the autoradiographic DG technique [13, 14]. It is important to understand that the transport of FDG and the enzyme mediated reactions are distinct from those for glucose. In order to estimate MRglc, however, the competitive kinetics between FDG and glucose must be taken into account.

In a 3-compartmental model (Fig. 13.4), C_1 represents FDG in plasma, C_2 represents free FDG in tissue, and C_3 represents FDG-6-phosphate. The basis for using FDG as a tracer to measure FDGglc is because FDG-6-phosphate is not a substrate for further metabolism, unlike glucose-6-phosphate. As a result, with FDG, only the transport and phosphorylation steps are incorporated into this model and not the remaining steps as in glycolysis. To calculate MRglc, however, measurement of the plasma glucose concentration (C_a^o) is needed to estimate intracellular glucose levels. A *lumped constant* (LC) was introduced to correct the differences in the in vivo behavior of FDG and glucose. The actual value of LC may vary (0.4–0.8) depending on the tissue (brain, myocardium, tumor) or plasma glucose levels. Based on the measured rate constants for FDG, LC, and (C_a^o), the MRglc can be calculated, at steady state, using the following equations:

$$\text{MRglc} = \left(\frac{K_1 \; k_3}{k_2 + k_3}\right)\frac{C_a^0}{LC} \tag{13.14}$$

$$\mathrm{MRglc} = K^{?}\frac{C_a^0}{LC} \tag{13.15}$$

Since arterial blood sampling is not practical in routine clinical applications, several different approaches have been developed to measure MRglc [1, 8, 15]. The Patlak plot is one approach that is based on a graphical method, which estimates the influx rate constant, K_1^* using only the time-activity data of dynamic FDG-PET images [16].

Receptor Binding

The dynamics of receptor binding studied by PET and SPECT imaging techniques can be analyzed using the 3-compartmental model (Fig. 13.4). In this model, C_a represents the unmetabolized free radioligand in the blood, C_f (or C_2) represents both the free, and the nonspecifically bound radioligand, and finally C_b represents only the receptor bound radioligand. The transfer of receptor binding radioligand in a 3-compartment model can be described using the differential equations, shown above (13.13 and 13.14), in which C_2 represents the free (nonspecifically bound) radioligand, while C_3 represents C_b, the receptor bound radioligand. The rate constant K_1, k_2, k_3 and k_4 are defined as delivery, washout, forward receptor-ligand reaction, and reverse receptor–ligand reaction, respectively. Many of the neuroreceptor ligands are lipophilic and may have nonspecific protein binding in blood or in tissue. Therefore, the fraction of the free ligand in the plasma (f_1) and the fraction of the free ligand in the tissue (f_2) that is available for specific receptor binding are important in the calculations.

Unlike the radiotracers that undergo metabolism, with the receptor binding radioligands, SA of the radioligand is very important. Since an unlabeled ("cold") ligand is present in the preparations of many radioligands, the cold ligand competes for the specific receptor binding sites with the labeled radioligand. Therefore, k_3 is very much dependent on the SA of the radioligand, as shown below:

$$k_3(t) = k_{on} f_2\left(B_{max}\,?\frac{C_b}{SA}\right) \tag{13.16}$$

In the above equation, if the SA is high, then C_b/SA (occupancy of receptors by the labeled compound) is negligibly small, and $k_3 \approx k_{on}.f_2.B_{max}$. If the receptor occupancy by the radioligand cannot be disregarded, k_3 is not constant, and the individual variables and constants must be determined separately by compartmental analysis, complicated curve-fitting, and analytic procedures. The clinical imaging studies would then require multiple radioligand injections with different SAs in order to determine the receptor density, $B_{max,}$ or affinity, K_D [17].

In routine clinical PET or SPECT neuroreceptor imaging studies, with a single radioligand, one can only determine the BP, which is B_{max} relative to K_D. (BP = B_{max}/K_D). Also, to prevent saturation effects, the intravenously administered radioligand should preferably bind to only a small fraction (<5%) of all the available receptor sites. Therefore, it is essential that the radioligand must be prepared in high SA (>1.0 Ci μmol^{-1}) so that the total mass of the ligand administered (labeled + cold ligand) is minimal. Very high SA is especially desirable when the receptor concentration is low, or when the radio labeled agonists are used to image high affinity receptor states. Under these conditions, the BP is related to the kinetic constants and can be estimated based on the following equation:

$$BP = \left(\frac{k_1\ k_3}{k_2\ k_4\ f_1}\right) \tag{13.17}$$

Under equilibrium conditions,

$$\left(\frac{k_1\ k_3}{k_2\ k_4\ f_1}\right) = \frac{C_b}{f_1 C_p} \tag{13.18}$$

The equilibrium *distribution volume* (DV or *V*) of compartment C_i is defined as the ratio of the tracer concentration in this compartment to the free arterial concentration (f_1C_f) at equilibrium. With neuroreceptor imaging studies, we have

$$V_2 = \frac{C_t}{f_1 C_p}; \quad V_3 = \frac{C_b}{f_1 C_p}; \quad V_T = V_2 + V_3 \qquad (13.19)$$

V_3, in the above equation, is the closest PET and SPECT equivalent of BP (BP = B/F), discussed under classical in vitro conditions, as shown in Eq. 13.8. While C_3 represents the receptor bound activity (B), the product $f_1 C_p$ represents the free ligand activity in plasma (L) [8, 9]. BP was originally defined as a ratio of B_{max}/K_D (based on in vitro receptor binding studies) or k_3/k_4 (based on kinetic parameters) [18].

The determination of BP based on the equation for V_3, described above, does require an arterial input function based on blood samples to determine (a) the free concentration of the radioligand (C_p) in plasma and (b) the free fraction in plasma (f_1). At equilibrium, the free radioligand concentration in plasma ($f_1 C_p$) can be assumed to be equal to the free radioligand concentration in the tissue ($f_2 C_t$). Since a reliable f_1 measurement is difficult to obtain for many tracers, the term f_1 is often neglected and assumed to be a constant across subjects. This leads to a more practical definition of BP and V_3 denoted here BP and V'_3 [9]:

$$BP = V_3 = \frac{C_b}{f_1 C_p} = \mathrm{BP}' = V_3' = \frac{C_b}{C_p} \qquad (13.20)$$

In order to avoid blood samples, one can also assume that a reference tissue compartment ($C_{t,ref}$) represents both free radioligand and nonspecifically bound radioligand. Now, at equilibrium, the BP can be expressed relative to the free and nonspecific binding in a reference tissue region such as the cerebellum ($C_3/C_{t,ref}$) [8, 9], as shown below:

$$\mathrm{BP}' = V_3' = \frac{C_b}{C_p} = BP' = V_3' = \frac{V_3}{V_2} = \frac{C_b}{C_{t,ref}} \qquad (13.21)$$

13.2.2.3 Graphical Analysis Methods

Graphical analysis (GA) techniques are simple methods for the analysis of data from radiotracer PET and SPECT imaging studies. In the initial evaluation of new radiotracers, they provide a visual way to distinguish between reversible and irreversible types of binding. They also provide considerable ease of computation compared to the optimization of individual model parameters in the solution of the differential equations generally used to describe the binding of radiotracers. GA methods are based on reformulating the model equations so that a linear relationship exists between the data and some quantitative parameter describing the nature of radio tracer binding or metabolism. These methods, however, do require an arterial input function although in some instances a reference region devoid of specific binding sites can be used in place of the plasma input function.

Patlak Plot

The theoretical foundation of GA for irreversible tracers was first developed and applied initially for the estimation of MRglc from dynamic FDG-PET data [16, 19]. The method is based on performing linear regression on the total tissue concentration (C'_p) divided by the plasma concentration at time (C'_T), as a function of the integral of the plasma concentration divided by the plasma concentration at time t (Table 13.1). The Patlak equation predicts that if one plots:

$$\frac{C'_T(t)}{C'_P(t)}\left(y\,?\,\text{axis}\right) \quad vs. \quad \frac{?_0^t C'_P(t)\,dt}{C'_P(t)}\left(x\,?\,\text{axis}\right) \qquad (13.22)$$

Table 13.2 Plasma and brain tissue time-activity data[a] following administration of [^{18}F]FDG

Time	Plasma	Time	Tissue		
min	nCi/mL	min	nCi/mL	$\frac{C_T^?(t)}{C_P^?(t)}$	$\frac{?_0^t C_P^?(t)dt}{C_P^?(t)}$
0.28	0.02	0.23	0.0	0	0
0.73	201	1.23	33	0.5	0.03
0.98	1150	2.23	96	2.3	0.13
1.48	1454	3.48	125	6.3	0.33
1.95	832	5.48	145	13	0.64
2.97	478	8.98	155	34	1.47
3.47	379	17.48	158	103	3.9
4.97	249	27.48	163	210	7.64
7.97	120	37.48	168	336	12.15
11.95	62	47.48	172	462	16.64
19.95	31	57.48	175	641	23.03
29.95	18	67.48	177	819	29.36
39.95	12	77.48	179	1028	36.82
59.97	7	87.48	180	1368	48.92
89.95	3.4	97.48	181	1694	60.55
119.95	1.8	112.48	182	2329	83.13

[a]The above simulated data is reproduced from [20]

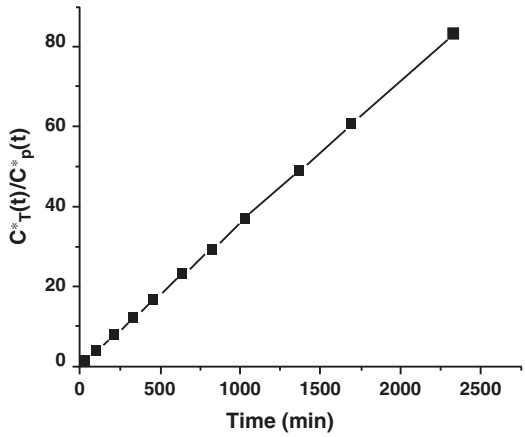

Fig. 13.5 The Patlak equation predicts that after some time $t > t^*$, a plot of total tissue concentration ($C_p^?$) divided by the plasma concentration at time ($C_T^?$) as a function of the integral of the plasma concentration divided by the plasma concentration at time t becomes linear. The plot based on data from Table 13.2 shows that the slope K^* is 0.036 [20]

The plot (Fig. 13.5) becomes linear over time with a slope of K^* (the influx constant) describing the transfer of the tracer from the plasma compartment to the irreversible compartment. It is important to note that K^* is dependent both on the binding or trapping rate and on the transport rate constants, K_1 and k_2. The Patlak plot is applicable for radiotracers that are metabolically trapped (FDG, FLT, FDOPA) but, not for receptor binding radioligands.

Logan Plot

Based on the original work of Patlak, the GA for reversible receptor binding radiotracers was initially developed by Logan [21, 22] and further refinements were proposed by Ichise [23, 24]. In the Logan plot, the integral of the ROI activity over the current ROI activity in the receptor binding tissue is plotted versus the integral of the plasma activity over the current ROI in the receptor binding tissue.

$$\frac{?_0^t C_t(?)d?}{C_t(t)}(y?\text{axis}) \quad vs. \quad \frac{?_0^t C_p(?)d?}{C_t(t)}(x?\text{axis}) \tag{13.23}$$

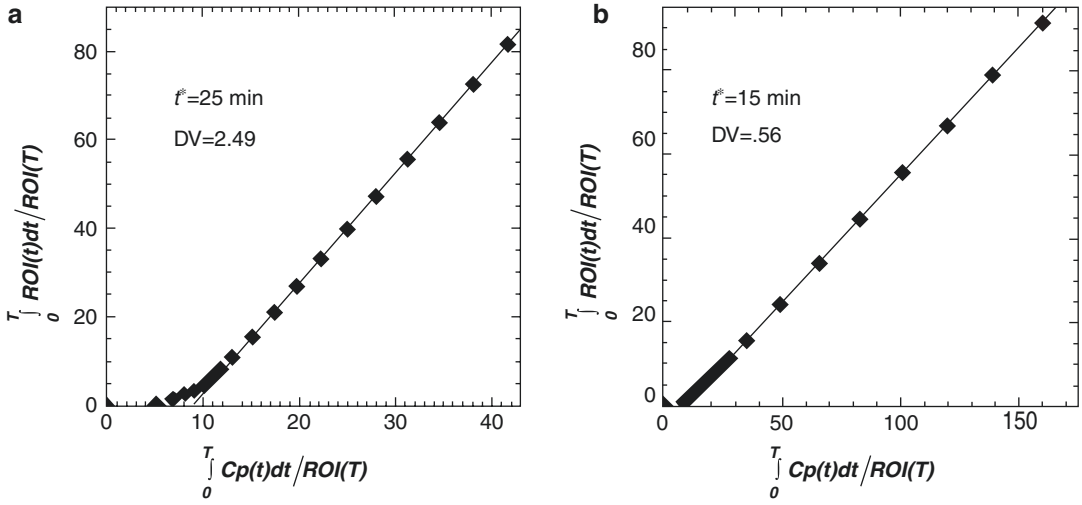

Fig. 13.6 Logan plots of graphical analysis: Time constant for start of the linear analysis for the basal ganglia is 25 min (**a**) and for the cerebellum it is 15 min (**b**). The shorter time for the cerebellum is due to its more rapid kinetics

The plot (Fig. 13.6) eventually becomes linear with a slope equal to the total radioligand volume of the distribution (V_T). The time to reach linearity (equilibrium), however, depends on the number of compartments and the nature of the radioligand.

The GA can be extended to obtain a distribution volume ratio (DVR) directly without blood sampling by using a tissue reference region (T_{ref}) instead of the plasma integral. This can be done by rearranging the GA equation for the T_{ref} to solve for the plasma integral in terms of the T_{ref} radioactivity. Based on the Logan plots, DV_{rec} and DV_{ref} tissue regions can also be determined separately in order to calculate the distribution volume ratio (DVR). Then the BP is given by

$$BP? \left(\frac{VD_{rec}}{VD_{ref}} \right) ?1 = DVR?1 \qquad (13.24)$$

References

1. Acton PD, Zhuang H, Alavi A. Quantification in PET. Radiol Clin North Am. 2004;42:1055–62.
2. Hofheinz F, Apostolova I, Oehme L. Test–retest variability in lesion SUV and lesion SUR in ^{18}F-FDG PET: an analysis of data from two prospective multicenter trials. J Nucl Med. 2017;58(11):1770–5.
3. Huang S. Anatomy of SUV: standardized uptake value. Nucl Med Biol. 2000;27:643–6.
4. Kinahan PE, Fletcher JW. PET/CT standardized uptake values (SUVs) in clinical practice and assessing response to therapy. Semin Ultrasound CT MR. 2010;31(6):496–505.
5. Zasadny KR, Wahl RL. Standardized uptake values of normal tissues at PET with 2-[fluorine-18]-fluoro-2-deoxy-D-glucose: variations with body weight and a method for correction. Radiology. 1993;189:847–50.
6. Michaelis L, Menten ML. Die Kinetik der Invertinwirkung. Biochem Z. 1913;49:1333.
7. Farde L, Eriksson L, Blomquist G, et al. Kinetic analysis of central [^{11}C]raclopride binding to D2-dopamine receptors studied by PET: a comparison to the equilibrium analysis. J Cereb Blood Flow Metab. 1989;9:696–708.
8. Ichise M, Meyer JH, Yonekura Y. An introduction to PET and SPECT neuroreceptor quantification models. J Nucl Med. 2001;42(5):755–63.
9. Laruelle M, Slifstein M, Huang Y. Relationships between radiotracer properties and image quality in molecular imaging of the brain with positron emission tomography. Mol Imaging Biol. 2003;5:363–75.
10. Lassen NA, Ingvar DH, Skinhoj G. Brain function and blood flow. Sci Am. 1978;239:62–71.
11. Raichle ME, Martin WR, et al. Brain blood flow measured with intravenous [^{15}O]H_2O. II. Implementation and validation. J Nucl Med. 1983;24:790–8.
12. Crone C. Permeability of capillaries in various organs as determined by the indicator diffusion method. Acta Physiol Scand. 1964;58:292–305.

13. Phelps ME, Huang SC, Hoffman EJ, et al. Tomographic measurement of local cerebral glucose metabolic rate in human with [^{18}F]2-fluoro-2-deoxyglucose. Validation of method. Ann Neurol. 1979;6:371–88.
14. Sokoloff L, Reivich M, Kennedy C, et al. The [^{14}C] de-oxyglucose method for the measurement of local cerebral glucose utilization: theory, procedure, and normal values in the conscious and anesthetized albino rat. J Neurochem. 1977;28:897–916.
15. Mankoff DA, Muzi M, Krohn KA. Quantitative positron emission tomography imaging to measure tumor response to therapy: what is the best method? Mol Imaging Biol. 2003;5:281–5.
16. Patlak CS, Blasberg RG, Fenstermacher JD. Graphical evaluation of blood-to-brain transfer constants from multiple-time uptake data. J Cereb Blood Flow Metab. 1983;3(1):1–7.
17. Heiss W-D, Herholz K. Brain receptor imaging. J Nucl Med. 2006;47:302–12.
18. Mintun MA, Raichle ME, Kilbourn MR, et al. A quantitative model for the in vivo assessment of drug binding sites with positron emission tomography. Ann Neurol. 1984;15:217–27.
19. Patlak CS, Blasberg RG. Graphical evaluation of blood-to-brain transfer constants from multiple-time uptake data. Generalizations. J Cereb Blood Flow Metab. 1985;5(4):584–90.
20. Gambhir SS. Quantitative assay development for PET. In: Phelps ME, editor. PET molecular imaging and its biological applications. New York: Springer; 2004.
21. Logan J. Graphical analysis of PET data applied to reversible and irreversible tracers. Nucl Med Biol. 2000;27(7):661–70.
22. Logan J. A review of graphical methods for tracer studies and strategies to reduce bias. Nucl Med Biol. 2003;30:833–44.
23. Ichise M, Fujita M, Seibyl J, et al. Graphical analysis and simplified quantification of striatal and extrastriatal dopamine D2 receptor binding with [^{123}I]epidepride SPECT. J Nucl Med. 1999;40:1902.
24. Logan J, Fowler J, Volkow N, et al. Graphical analysis of reversible radioligand binding from time-activity measurements applied to [N-^{11}C-methyl]-(−)-cocaine PET studies in human subjects. J Cereb Blood Flow Metab. 1990;10:740–7.